Available online at www.sciencedirect.com
ScienceDirect
Deep-Sea Research II 54 (2007) 2630–2642
DEEP-SEA RESEARCH PART II
www.elsevier.com/locate/dsr2

The impact of bio-optical heating on the properties of the upper ocean: A sensitivity study using a 3-D circulation model for the Labrador Sea

Yongsheng Wu[a,b], Charles C.L. Tang[a,*], Shubha Sathyendranath[b,c], Trevor Platt[a]

[a]*Bedford Institute of Oceanography, Fisheries and Oceans Canada, Dartmouth, NS, Canada B2Y 4A2*
[b]*Department of Oceanography, Dalhousie University, Halifax, NS, Canada B3H 4J1*
[c]*Plymouth Marine Laboratory, Prospect Place, The Hoe, Plymouth PL1 3DH, United Kingdom*

Received in revised form 18 January 2007; accepted 4 August 2007
Available online 17 October 2007

Abstract

The impact of bio-optical heating on the properties of the upper Labrador Sea water was investigated by considering changes in light attenuation in water associated with the seasonal change of chlorophyll distribution. The time- and depth-dependent attenuation coefficients were obtained from remotely sensed SeaWiFS ocean-colour data. Sea-surface temperature (SST) and mixed-layer depth (MLD) were computed from a three-dimensional ocean circulation model. The model was integrated from 1999 to 2003 with 6-hourly atmospheric forcing. The changes in SST and MLD attributable to bio-optical heating were determined by comparing the model results using the observed attenuation coefficients (chlorophyll) to those using a weak and constant attenuation (clear water). The model results show that bio-optical heating is controlled mainly by chlorophyll concentration and MLD. The increase in SST is around 1 °C in most parts of the Labrador Sea and the shelves, and up to 2.7 °C in areas of shallow MLD and high chlorophyll concentrations (the Grand Banks and Northeastern Newfoundland Shelf). The increase is much higher than that found in previous studies, which was typically a fraction of a degree. Bio-optical heating also can enhance the stratification of the upper ocean and reduce the MLD by 20–50%.

Keywords: Biological heating; Chlorophyll distribution; Labrador Sea; Optical property; Upper layer dynamics

1. Introduction

Mixed-layer models seek to find the depth and temperature of the mixed layer through assessing the balance between the opposing tendencies of the ocean to stratify under surface heating and freshening and to mix under the influence of wind. Thus, all such models require a description of the solar heating of the ocean. The solar energy reaching the surface of the ocean may be divided into two components: called non-penetrating and penetrating. The former accounts for the infrared radiation, which is attenuated so strongly by water that it penetrates less than a few centimetres. The latter accounts for the visible radiation, to which the ocean is not spectrally neutral, and which penetrates

*Corresponding author. Tel.: +1 902 426 2960; fax: +1 902 426 6927.
E-mail address: TangC@mar.dfo-mpo.gc.ca (C.C.L. Tang).

0967-0645/$ - see front matter © 2007 Elsevier Ltd. All rights reserved.
doi:10.1016/j.dsr2.2007.08.019

to a greater or lesser extent depending on the materials present in the ocean, either in solution or in suspension. The penetration is parameterised by the vertical attenuation coefficient K, with dimensions $[L^{-1}]$ or, strictly, $K(\lambda)$, where λ is the wavelength, and is calculated using a bio-optical model (Sathyendranath and Platt, 1988, 1997, 1998).

For the non-penetrating component of solar radiation, attenuation is taken as infinite; this component is attenuated at the surface. For the penetrating component, K has been specified in different ways. For example, McCreary and Kundu (1989) took K to be infinite. Niiler and Kraus (1977) considered K to be finite but globally constant. Paulson and Simpson (1977) assigned a K value according to the Jerlov system of optical water types (Jerlov, 1976). Denman (1973) achieved good agreement between model and observations for Station P in the Pacific Ocean only if he tuned K.

Tuning raises the question of potential causes of the change of K in the ocean. In the open ocean, the principal factor controlling K is the local phytoplankton biomass: its effect on K arises from the cell pigments, usually indexed as the chlorophyll concentration. The dynamic range of chlorophyll concentration in the ocean is four orders of magnitude, such that there is considerable scope for variation of K with season and location. This is the explanation for the experience of Denman (1973), whose work was conducted in the spring, when chlorophyll concentrations are at the highest for the year. Given the potential for variation in K with chlorophyll concentration, one might expect that mixed-layer models would be more likely to succeed if K were prescribed as a function of local chlorophyll concentration. Two broad options exist to accomplish this.

The first option is to couple the physical model to an ecosystem model that would update the chlorophyll concentration with the same integration time step as the physical model. An early example is Simonot et al. (1988), wherein the chlorophyll concentration was updated in the ecological model, but K was not calculated from chlorophyll. This model might be described as partially coupled. Perhaps the first fully coupled models were those of Platt et al. (1994a) and Sathyendranath and Platt (1994), where a simple ecological model simulated the seasonal change in chlorophyll concentration, which was then used to derive the time variation in K for application in the mixed-layer model.

The second option is to use remotely sensed images of ocean colour, which provide surface chlorophyll concentration on synoptic scales. These data can be assimilated into mixed-layer models, and their effects on the model results, e.g., sea-surface temperature (SST) and mixed-layer depth (MLD), can be examined by comparing the effect of a bio-optical K (hereinafter referred to as K_{var}) with that of a constant K for clear water (hereinafter referred to as K_{const}). This effect on the model predictions may be considerable as has been demonstrated for the Arabian Sea (Sathyendranath et al., 1991). They show that the maximum biologically induced heating warmed the surface water by 4 °C from August to September 1979. This approach was followed in a variety of studies using three-dimensional (3-D) ocean models. For example, Nakamoto et al. (2000) showed the SST increased by up to 0.6 °C and the MLD decreased by 20 m. Shell et al. (2003) discussed the atmospheric implication of the biological heating and concluded that the SST increased 0.3 °C globally and might reach 1 °C locally. Similarly, Manizza et al. (2005) concluded that the presence of phytoplankton warmed SST by 0.1–1.5 °C in spring and summer at mid and high-latitudes using a global model. In most models, a constant K was used in the mixed layer. In the Labrador Sea, the attenuation scale derived from remotely sensed data for the Labrador Sea water is of the order $1/K$ ~5–10 m, which is smaller than a typical MLD of ~20 m in summer. In assessing the impact of bio-optical heating, one should therefore consider the variation of K within the mixed layer itself.

There have been many studies of the bio-optical contribution to upper dynamics in equatorial waters, but few in other regions, especially in high-latitude waters. The Labrador Sea is a region with strong seasonal dynamics and important spatial gradients in the phytoplankton. Moreover, there is significant interannual variability between years in the ecological dynamics.

Here, we apply the second option (assimilation of ocean-colour data) to an existing circulation model of the Labrador Sea (Yao et al., 2000). To examine the impact of K_{var} on the upper ocean, we compare the results from the model employing: (a) K_{var} from Sathyendranath and Platt's (1988) spectral bio-optical model and ocean-colour data; and (b) K_{const} used in most contemporary ocean circulation models. Chlorophyll is not a variable of the model. Its impact on the ocean properties is studied

through K in the temperature equation. The focus of the paper is the mixed-layer temperature (or SST) and MLD. Observations and modeling studies show that SST and MLD are controlled not only by solar radiation but also by surface heat fluxes, wind mixing and stability of the water column. In regions of strong currents, horizontal advection is also important. To isolate the effects of light attenuation in our model experiments, we use the same surface heat fluxes, wind stress and initial temperature-salinity fields, but different K.

2. Model and data description

2.1. Ocean model

The numerical model used for this study is similar to the model described by Yao et al. (2000), which is based on the Princeton Ocean Model (POM; Blumberg and Mellor, 1987) coupled to a sea-ice model. The main difference between the Yao et al. (2000) model and the present model is the incorporation of the generalised vertical coordinate system (Ezer and Mellor, 2004). The new coordinate system is necessary because the minimum MLD in the study area is less than 20 m and the attenuation scale of the penetrating solar radiation is ~10 m. The upper ocean could not be resolved adequately if the conventional sigma coordinate system (vertical level intervals are fixed percentages of the water depth) were used. The generalised vertical coordinate system permits a z-level representation everywhere in the model domain independent of the water depth. The coordinate system used in our model has 30 vertical levels consisting of 10 constant z-levels (2 m) and 20 sigma levels.

The model domain is from Davis Strait to the Gulf Stream and from the Canadian east coast to 40°W with a horizontal resolution of approximately 20 km × 20 km (Fig. 1). The open boundary conditions were prescribed according to Yao et al. (2000). Model initialisation and spin up followed the procedures in that paper.

2.2. Ocean data, atmospheric forcing and heat fluxes

3-D ocean temperature and salinity data are required for model initialisation and SST assimilation. Available global-scale datasets may not be suitable for the present study because the data resolution is not compatible with the model resolution. In this study, the monthly temperature and salinity climatologies obtained from an objective analysis of the hydrographic data archived at Bedford Institute of Oceanography were used (Tang and Wang, 1996).

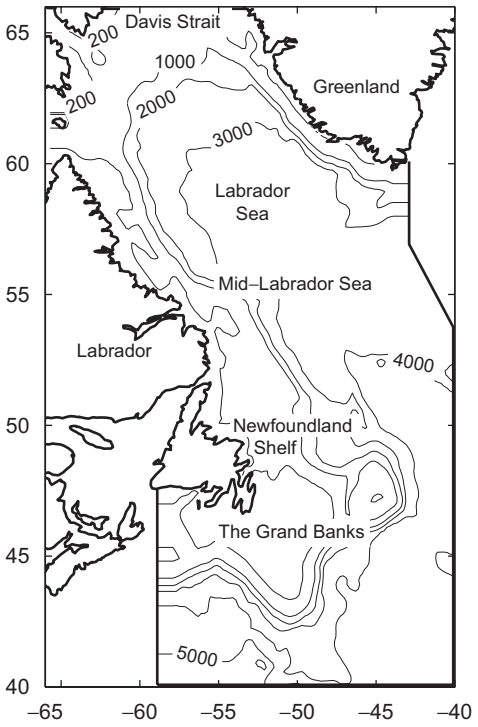

Fig. 1. Map showing the model domain (heavy line) and topography. The solid circles are the sites in the Labrador Sea and the Grand Banks used in Figs. 6–10.

Six-hourly meteorological data including air temperature, specific humidity, precipitation, cloud fraction and 10 m wind from NCEP/NCAR Reanalysis-2 (Kalnay et al., 1996) were used to compute the atmospheric forcing. The calculations of the total downward irradiance at the surface, $Q_{SOL}(0)$, latent heat (Q_{LAT}), sensible heat (Q_{SEN}) and long wave radiation (Q_{LW}) follow the methods in Yao et al. (2000). The sign convention is positive for upward fluxes (solar radiation is always negative).

2.3. Optical models

In general, two types of optical models are commonly used in ocean circulation models. The first is the well-known Jerlov's "water types" model due to its simplicity and computational efficiency (Jerlov, 1976; Paulson and Simpson, 1977). Six water types are defined according to their optical properties and two constant attenuation coefficients assigned to each water type. The other is bio-optical

models in which the attenuation coefficient is calculated from observed chlorophyll concentration (e.g., Sathyendranath and Platt, 1988; Morel, 1988; Platt et al., 1994b).

2.3.1. Water type model

In the Paulson and Simpson (1977) model, the downward irradiance is formulated with two extinction depths λ_1 and λ_2 ($\lambda_1 \ll \lambda_2$) corresponding to the Jerlov water type classification. Its general form is given as:

$$Q_{\mathrm{SOL}}(z) = Q_{\mathrm{SOL}}(0)[R\mathrm{e}^{z/\lambda_1} + (1-R)\mathrm{e}^{z/\lambda_2}]. \quad (1)$$

The first term on the right describes the rapid attenuation of the red spectral component within the top centimetres; the second term describes the much weaker attenuation of blue-green spectral components, and hence this component penetrates much deeper. z is the vertical coordinate (positive upward). The empirical constant, R, is the fraction of the total surface radiation that does not penetrate the surface. Let Q_{pen} and Q_{npen} represent, respectively, the penetrating and non-penetrating components of the solar radiation. The relation between Q_{SOL}, Q_{pen} and Q_{npen} is approximately:

$$\begin{aligned} Q_{\mathrm{SOL}}(z) &= Q_{\mathrm{npen}}(z) + Q_{\mathrm{pen}}(z) \\ &= Q_{\mathrm{npen}}(0)\mathrm{e}^{z/\lambda_1} + Q_{\mathrm{pen}}(0)\mathrm{e}^{z/\lambda_2}, \\ Q_{\mathrm{npen}}(0) &= RQ_{\mathrm{SOL}}(0), \\ Q_{\mathrm{pen}}(0) &= (1-R)Q_{\mathrm{SOL}}(0). \end{aligned} \quad (2)$$

The quantity $Q_{\mathrm{pen}}(z)$ heats the water column and is the source term for the temperature equation:

$$\frac{\partial T}{\partial t} + \mathbf{u}\nabla T + w\frac{\partial T}{\partial z} = \frac{\partial}{\partial z}\left(K_{\mathrm{H}}\frac{\partial T}{\partial z}\right) + F_{\mathrm{T}} - \frac{1-A}{\rho_0 c_{\mathrm{p}}}\frac{\partial Q_{\mathrm{pen}}}{\partial z}, \quad (3)$$

where K_{H} is the vertical eddy diffusivity, F_{T} represents horizontal diffusion, c_{p} is the heat capacity, ρ_0 is the seawater density and A is the ice concentration, which varies from 0 (no ice) to 1 (complete ice cover). For $A = 1$, no penetrating solar radiation can reach the water surface.

Since Q_{npen} is absorbed within the top centimetres of the water column, it can be treated as a boundary condition for temperature:

$$K_{\mathrm{H}}\frac{\partial T}{\partial z}\bigg|_{z=0} = \frac{1}{\rho_0 c_{\mathrm{p}}}(Q_{\mathrm{npen}}(0) + Q_{\mathrm{LW}} + Q_{\mathrm{LAT}} + Q_{\mathrm{SEN}} + Q_{\mathrm{CORR}}), \quad (4)$$

where Q_{CORR} is a flux correction term to restore SST to climatology. The detail of this term will be given in Section 2.4. This boundary condition applies to the ice-free part of the ocean only. For the ice-covered water, ice thermodynamics is considered and the heat flux between the ocean and sea-ice is computed using the ice-ocean coupling scheme of Mellor and Kantha (1989).

2.3.2. Bio-optical model and ocean-colour data

In the bio-optical model, a time- and space-dependent $K(z)$ is used. The second term of Eq. (1) is replaced by $Q_{\mathrm{SOL}}(0)(1-R)\mathrm{e}^{zK(z)}$. To determine $K(z)$, the average light attenuation coefficient from the surface to depth z, we used a regionally adapted version of the bio-optical model of Sathyendranath and Platt (1988). In this model, the wavelength-resolved attenuation coefficient for downwelling irradiance is expressed as a function of the total absorption coefficient (sum of absorptions by pure water, phytoplankton and yellow substances), the back-scattering coefficient (sum of back-scattering by pure water and particulate material), and the mean cosine for downwelling irradiance computed using an atmospheric light transmission model (Bird, 1984). The phytoplankton absorption was parameterised as a function of chlorophyll concentration using the two-population absorption model of Sathyendranath et al. (2001). The model was tuned to the Northwest Atlantic, by fitting it to pigment and absorption data from the region, for all wavelengths from 400 to 700 nm at 5-nm intervals. The absorption by pure water is modelled using values from Pope and Fry (1997). Back scattering and absorption by yellow substances are modelled as in Sathyendranath et al. (2001). Once the spectral light available at the sea surface is computed for a given location and time using an atmospheric light transmission model (Bird, 1984) modified for cloud effects (Platt et al., 1990), the spectral light available at depth z can be estimated using the Sathyendranath and Platt (1988) model, modified as described above. The light over the visible domain (400–700 nm) at the surface, $Q_{\mathrm{pen}}(0)$, and that at z, $Q_{\mathrm{pen}}(z)$, are then estimated by integrating the spectral irradiance over all wavelengths. The attenuation coefficient $K(z)$ for the penetrating component of the solar flux is then estimated as:

$$K(z) = \frac{1}{z}\ln\left(\frac{Q_{\mathrm{pen}}(z)}{Q_{\mathrm{pen}}(0)}\right). \quad (5)$$

Look-up tables of K were generated using light conditions for latitude 45°N, local noon and an arbitrary cloud cover of 50%, and for a range of discrete biomass values and depths. The model was implemented using chlorophyll-*a* computed using SeaWiFS data for the period from September 1997 to December 2001, processed into bi-weekly averages (1st–15th, 16th-month end) at each model grid node using the SeaDAS OC4v4 software package. The chlorophyll concentration derived from satellite data was assumed to be distributed uniformly within the layer from 0 to z. For each bi-weekly period and for each model grid point, values for $K(z)$ were obtained from the look up table by linear interpolation.

The chlorophyll concentrations used in the model simulations are 5-year averages of the bi-weekly data. The averaging is necessary to ensure that there is no data gap in the model domain. Fig. 2 shows the mean chlorophyll concentration from March to October. The salient feature is the increase in phytoplankton biomass during the spring bloom. Generally, this phenomenon progresses northward as the season advances, but note that off West Greenland the bloom develops early.

Fig. 3 shows the profiles of $K(z)$, $I(z) = Q_{\mathrm{pen}}(z)/Q_{\mathrm{pen}}(0)$ and $\partial I/\partial z$ for different chlorophyll concentrations and Water Type I. Temperature change attributable to biology is controlled by $\partial Q_{\mathrm{pen}}/\partial z$ according to Eq. (3). The right panel of Fig. 3 shows that the presence of chlorophyll increases the absorption of solar radiation in the top 5 m significantly.

2.4. Numerical experiments

The model was integrated from January 1, 1999 to December 31, 2003 (the period covered by biological data) with 6-hourly forcing. In multi-year model simulations, it is well known that applying

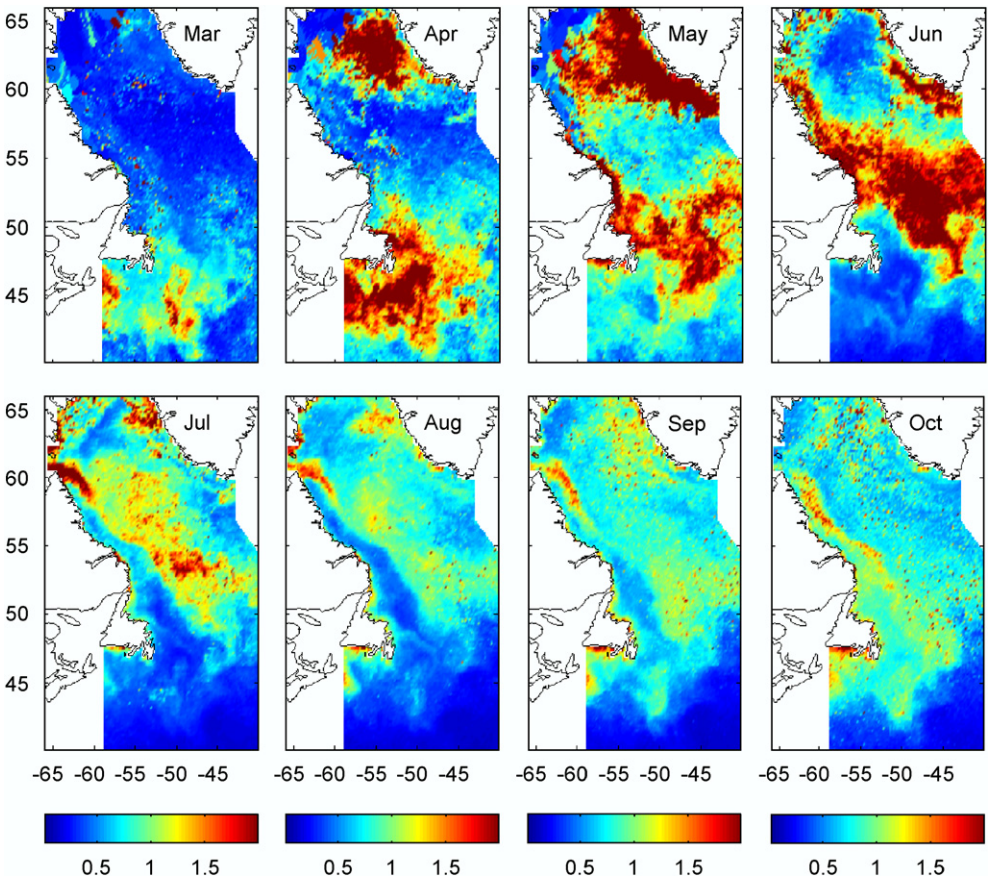

Fig. 2. Five-year averages of bi-weekly surface chlorophyll concentration in mg m^{-3} from March to October. Only the second bi-weekly averages for each month are shown.

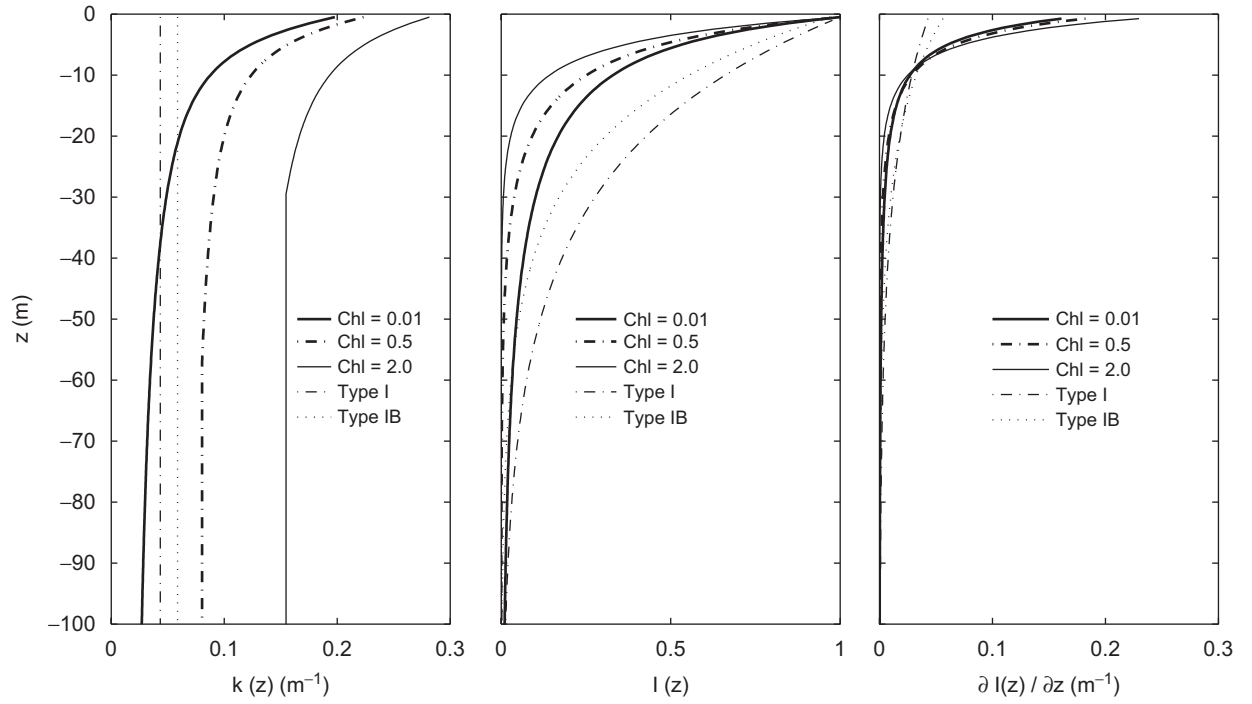

Fig. 3. Comparison of the attenuation coefficient $K(z)$ (left panel), downward irradiance normalised by the surface value $I(z) = Q_{pen}(z)/Q_{pen}(0)$ (middle panel), and the vertical gradient $dI(z)/dz$ (right panel) for different surface chlorophyll concentration (mg m^{-3}), Water Type I and IB. Note that the Jerlov water types give values of K that are non-spectral. This accounts for the differences in shape between the vertical profiles for these water types and the rest of the cases plotted, as well as the higher values of K at depth for pure water (Jerlov Water Type I) than for chlorophyll-a levels of 0.01 mg m^{-3}.

heat fluxes calculated from observed or climatological SST may lead to SST drift and other problems (Barnier, 1998; Rochford et al., 2001). To minimise the SST drift in our simulations, we follow the data assimilation method of Barnier (1998). The net surface heat flux, Q_{NET}, is written as the sum of the computed flux, Q_{SUR}, and a correction term, Q_{CORR}:

$$Q_{NET} = Q_{SUR} + Q_{CORR}, \tag{6}$$

$$Q_{SUR} = Q_{SOL}(0) + Q_{LW} + Q_{LAT} + Q_{SEN}, \tag{7}$$

$$Q_{CORR} = \left(\frac{\partial Q_{SUR}}{\partial T}\right)_{T_S^{Clim}} (T_S^{Clim} - T_S), \tag{8}$$

where T_S^{Clim} is the climatological SST and T_S is the model SST. The quantities Q_{LW}, Q_{LAT}, Q_{SEN} are functions of T_S^{Clim} and the 6-hourly atmospheric parameters. The correction term (8) can help to minimise the deviation of the model mean SST from T_S^{Clim}. Salinity is treated in a similar way as temperature.

We integrated the model for 5 years (1999–2003) with the flux correction term and $K_{var}(z)$ to obtain the daily mean heat and water fluxes. The impact of bio-optical heating on the upper-ocean layer is examined from the results of two numerical experiments using these fluxes: one with a variable $K_{var}(z)$ and the other with a constant K_{const} for Water Type I, i.e., $\lambda_2 = 23$ m. The same fraction of the penetrating irradiance, $1-R = 0.42$, was specified in the two experiments. It is important to note that, to isolate the effect of light attenuation, the model must be forced by the same surface fluxes but different attenuation coefficients (Martin, 1985). The SST assimilation by the flux-correction method as outlined above was applied to the K_{var} experiment only. As a result, the model SST from this experiment is close but not equal to the climatological SST. In the K_{const} experiment, the heat and fresh-water fluxes were prescribed (taken from the K_{var} experiment) and hence the model SST was not constrained by climatology. If flux corrections were also applied to the K_{const} experiment, the heat and water fluxes in the two experiments would be different. Alternatively, we could apply flux corrections to the K_{const} experiment and use the same fluxes for the K_{var} experiment. The model results

were averaged over the five years to represent the 5-year mean, which are shown in the following section.

In this study, we are not concerned with the dynamics of sea ice, and sea ice was not simulated in the model experiments. Climatological sea-ice data (ice concentration and thickness) provided by Canadian Ice Service were used in the model. The role of sea ice is to insulate the ocean from the atmosphere, and exchange heat and water with the underlying water through ice melt and growth. The inclusion of sea ice in the model reduced the ocean heat loss and kept the SST at the freezing point in the ice-covered part of the ocean.

3. Model results

3.1. Sea-surface temperature

The effect of bio-optical heating can be quantified by defining an SST difference, ΔSST, which is the SST from the K_{var} experiment minus SST from the K_{const} experiment. Fig. 4 shows SST for March, May, July and September from the K_{var} experiment. Large seasonal variations can be seen in the Labrador and Newfoundland shelves, the Grand Banks and the central Labrador Sea. The main SST features are the warm water of the Gulf Stream in the south, cold water along West Greenland and the Labrador coast, and intrusion of the relatively warm North Atlantic Water into the central Labrador Sea in summer.

The seasonal variation of MLD (see Section 3.3 for a discussion of the definition of MLD) has a very large range, 10–1000 m (Fig. 4). In winter and early spring, intense winds and surface cooling creates mixed layers thicker than 200 m in the open Labrador Sea except in ice-covered areas. The deepest mixed layer (>1000 m) appears in northern Labrador Sea just outside of the ice zone. Over the shallow (~70 m) Grand Banks, the water is mixed from top to bottom. Rapid shallowing of the mixed layer starts in early May reaching a minimum in July when the MLD is less than 20 m in the entire area.

Fig. 5 displays the monthly values of ΔSST, which are negligible in winter and largest from July to September. Starting from early June, the area of enhanced surface warming spreads from the Grand Banks to the Labrador Shelf and then expands to the central and northern parts of the Labrador Sea. The large annual variation of ΔSST appears to be related to both the chlorophyll concentration and MLD. A comparison of Figs. 2 and 5 reveals that

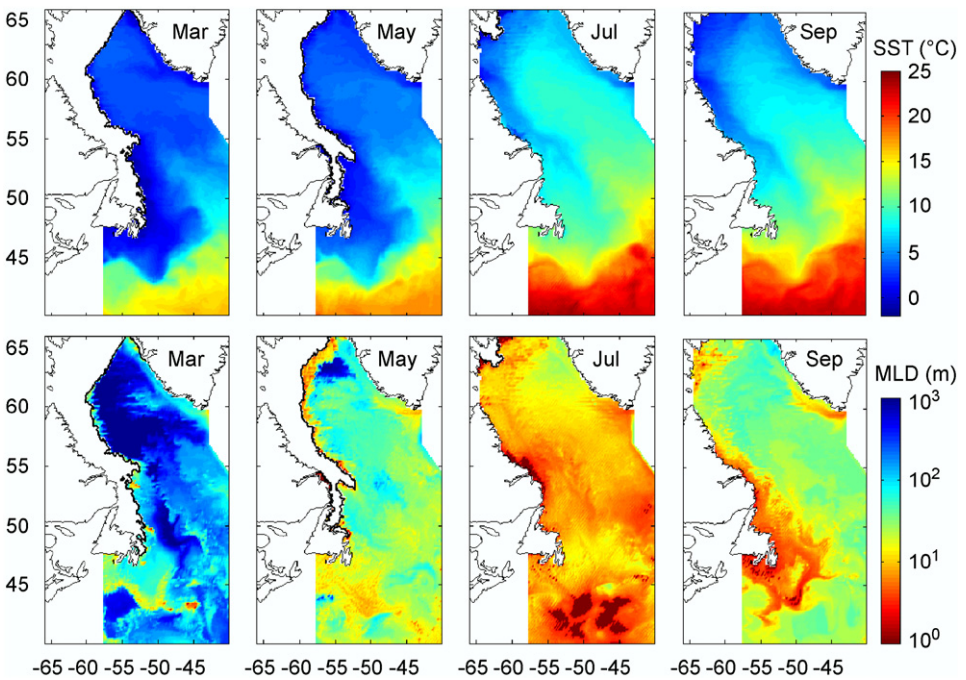

Fig. 4. Model SST (upper row) and MLD (lower row) for March, May, July and September from the K_{var} experiment. Ice cover in winter and spring off the Labrador coast is indicated in white. The scale is linear for SST and logarithmic for MLD.

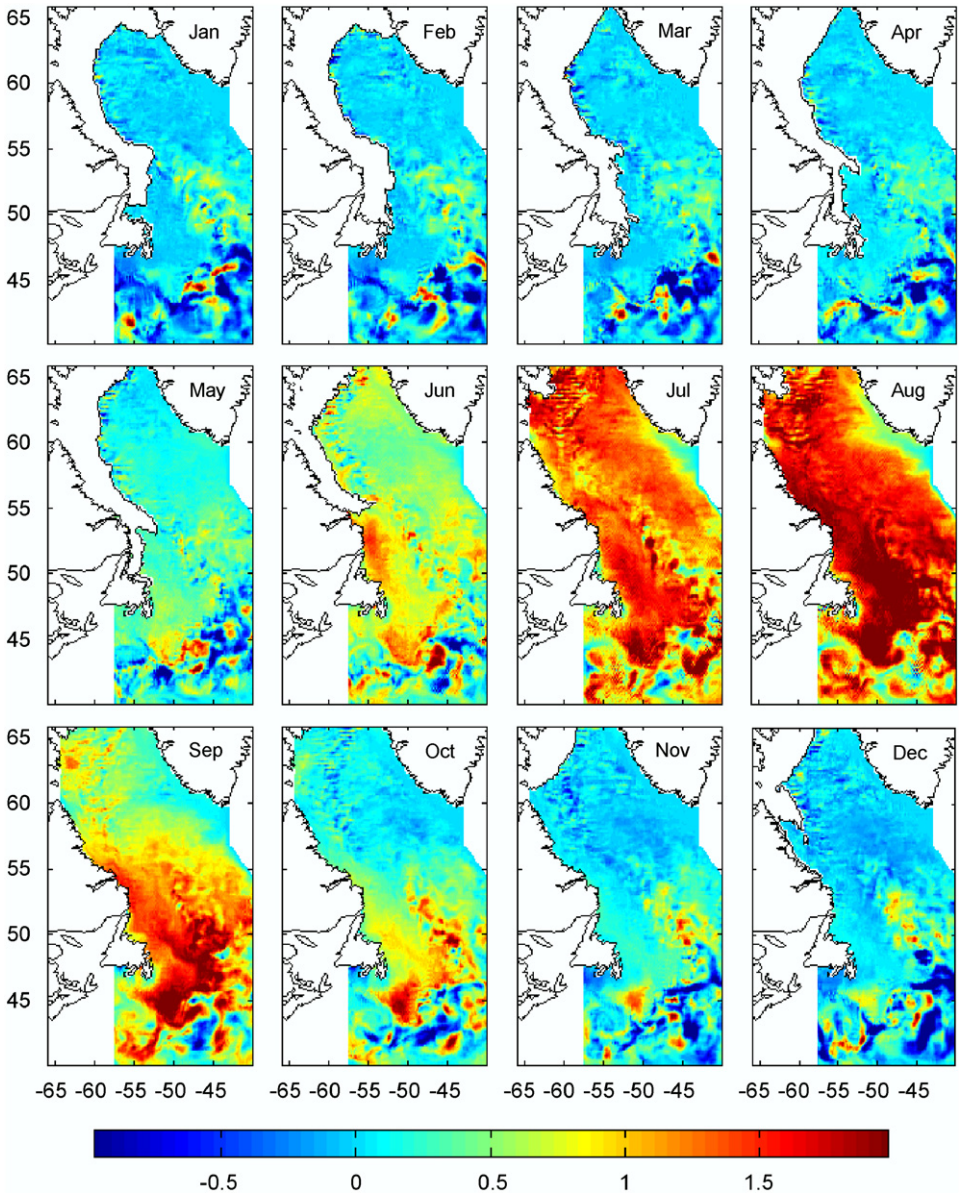

Fig. 5. Monthly model ΔSST from the K_{var} and K_{const} experiments. Ice cover in winter and spring off the Labrador coast is indicated in white. Some of the anomalies are negative. This counterintuitive result is a consequence of the non-spectral nature of the attenuation coefficient under the Jerlov water types, as mentioned in the caption of Fig. 3.

the areas of high chlorophyll concentration do not always have large ΔSST, for example the northern Labrador Sea in April and May. The MLD in northern Labrador Sea at this time is greater than 60 m. At this depth, Q_{pen} does not depend strongly on chlorophyll concentration or water type (see the middle panel of Fig. 3). Since ΔSST increases with the net solar flux in the mixed layer, $Q_{pen}(0)-Q_{pen}(-h)$ (h is the MLD), the small difference in Q_{pen} at the base of the mixed-layer between K_{var} and K_{const} results in a small ΔSST. On the other hand, the areas of low concentration of chlorophyll can have large ΔSST, e.g., the Grand Banks and Northeastern Newfoundland Shelf from June to August and the open Labrador Sea in August. During these periods, the MLD at the Grand Banks/Northeastern Newfoundland Shelf and the mid-Labrador Sea are about 10 and 25 m, respectively. At these depths, $Q_{pen}(-h)$ between K_{var} and K_{const} are significantly different even for low

chlorophyll concentrations. The large differences in K lead to large ΔSST. Further discussion on the relationship between solar heating and MLD will be given in Section 4.

The SST difference increases progressively from June, reaches a peak in August, and then decreases in autumn. The mean ΔSST is of the order 1.5–2 °C in summer. The regions of large ΔSST include the central Labrador Sea and the Grand Banks where the maximum ΔSSTs are 1.8 and 2.7 °C, respectively (Fig. 6). Water Type I represents "clear water", and the SST difference between K_{var} and Water Type I is usually defined as the net effect of phytoplankton on SST (Nakamoto et al., 2000; Shell et al., 2003; Manizza et al., 2005).

3.2. Vertical temperature variation

To study the effect of bio-optical heating below the surface, it is helpful to examine ΔT (temperature from K_{var} minus temperature from K_{const}) in the time-depth plane (Fig. 7). Warming in the upper water column and cooling in the lower water column are observed at both locations. The upper

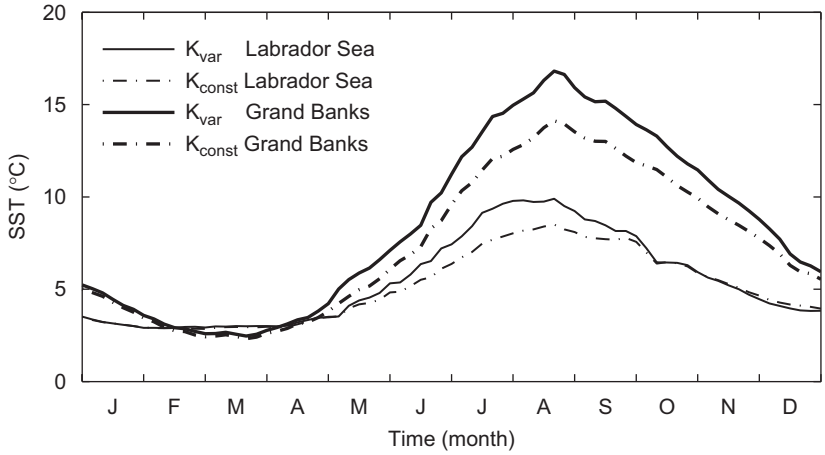

Fig. 6. Comparison of SST from the K_{var} and K_{const} experiments at mid-Labrador Sea and the Grand Banks (see Fig. 1 for locations).

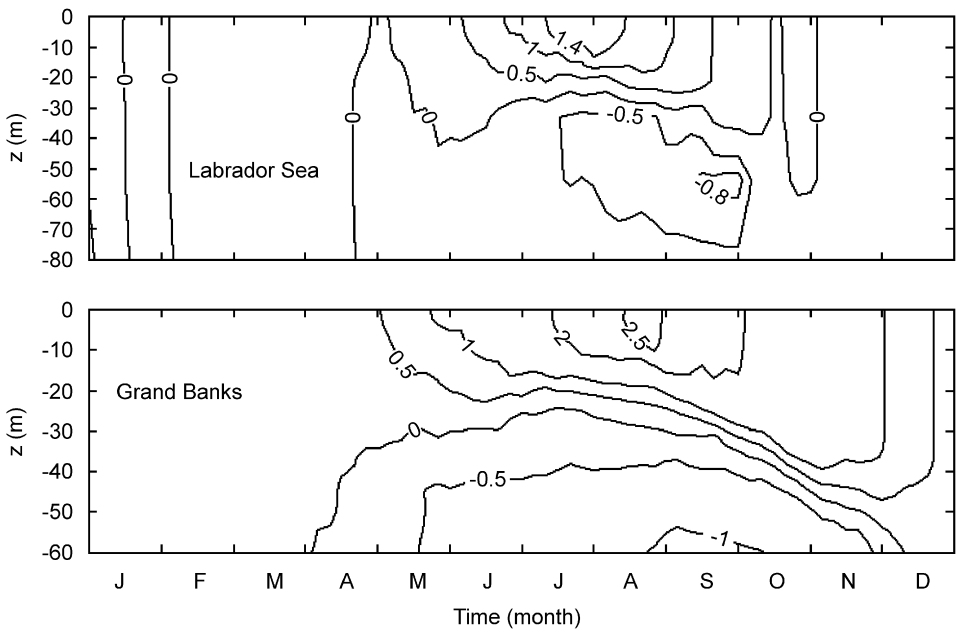

Fig. 7. ΔT in the depth–time plane for mid-Labrador Sea (upper panel) and the Grand Banks (lower panel) (see Fig. 1 for locations).

layer is warmed by the absorption of sunlight by phytoplankton pigments, whereas the lower-layer temperature decreases due to the reduction of solar radiation (see the right panel of Fig. 3). On the Grand Banks, the maximum temperature increase and decrease are around 2.7 and 1.2 °C, respectively. The depth and annual variation of the warming and cooling features in mid-Labrador Sea are similar to those on the Grand Banks, but the magnitudes of the temperature differences are smaller. The warming in the upper layer can change the stratification and reduce vertical mixing, which lead to a shallower mixed layer. This effect is examined in the following sub-section.

3.3. Mixed-layer depth

In the 3-D model used this study, ocean variables are computed at every grid point. Unlike the bulk mixed-layer models (Denman, 1973; Niiler and Kraus, 1977), the MLD is not a variable of the model and no assumption about the temperature and salinity distribution within the mixed layer is made. Here, the MLD is defined as the depth at which the density increase from the surface value, $\Delta\rho$, reaches 0.1 kg m^{-3}. Fig. 8 shows contours of $\Delta\rho$ at mid-Labrador Sea and the Grand Banks. In summer and fall, the closeness of the contour lines suggests that MLD is not sensitive to the value of $\Delta\rho$. From April to October, a sharp decrease in MLD occurs in April and May (Fig. 9). The mixed layer remains shallow through summer until September. Both at the Grand Banks and mid-Labrador Sea, the MLDs from K_{var} are in general smaller than the MLDs from K_{const}. During the summer period at mid-Labrador Sea, the average difference in MLD is about 10 m, i.e., the MLD from K_{var} is ~20–50% smaller than that from K_{const}. For the Grand Banks, the corresponding figures are 5 m and 25–40%.

4. Discussion

The K_{var} from Sathyendranath and Platt (1988, 1997, 1998) model gives an extinction depth of a few tens of meters (Fig. 3). Close to 90% of the penetrative irradiance is absorbed within the top 20 m. The small extinction depth suggests that model prediction could be sensitive to model resolution.

To examine the model sensitivity to vertical resolution, we modified the coordinate system of the model from a vertical resolution of 2–10 m in the upper water column and repeated the numerical experiments. The results show that in mid-Labrador Sea, ΔSST from the 10 m experiment is smaller than

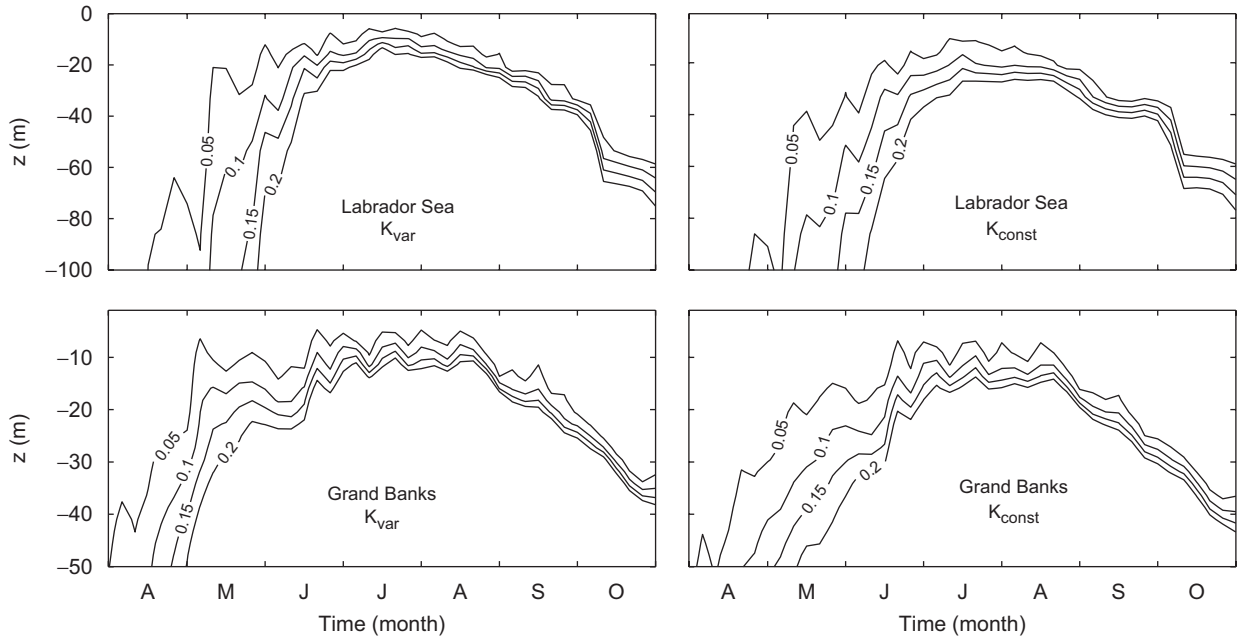

Fig. 8. Density difference from the surface values from the K_{var} (left panels) and K_{const} (right panels) experiments for mid-Labrador Sea and the Grand Banks. The contour interval is 0.05 kg m^{-3} (see Fig. 1 for locations).

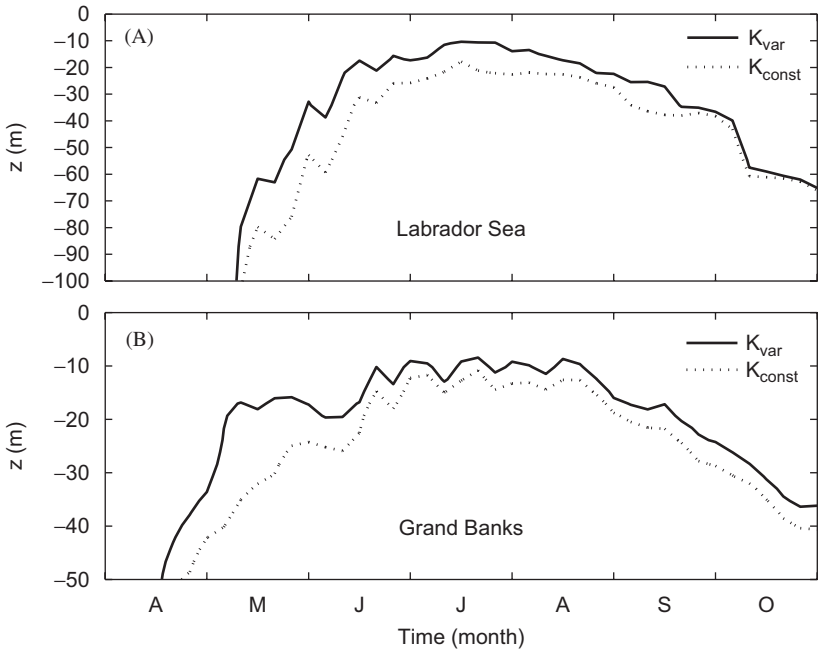

Fig. 9. Comparison of the mixed-layer depth from April to October for mid-Labrador Sea (upper panel) and the Grand Banks (lower panel) (see Fig. 1 for locations).

that from the 2 m experiment by about 0.43 °C in summer, which is about 32% of the ΔSST from the 10 m experiment. These results indicate that a coarse vertical resolution model for the Labrador Sea can lead to sizable errors.

The magnitude of ΔSST depends on how "clear water" is defined. To investigate the sensitive of ΔSST to water type, we repeated the numerical experiments with Water Type I replaced by Water Type IB which has an extinction depth, λ_2, of 17 m and $1-R = 0.33$. The maximum ΔSST is 0.92 °C for the Grand Banks and 0.90 °C for mid-Labrador Sea. In comparison with the results from Water Type I, ΔSST is smaller but still significant.

Our model experiments show that the biological contribution to ΔSST in the Labrador Sea is much larger than predictions from global models (Shell et al., 2003; Manizza et al., 2005), which give ΔSST typically a fraction of a degree. The large ΔSST in the Labrador Sea can be understood from a consideration of heat conservation in the mixed layer. The available Q_{pen} for the mixed layer is the difference between the incoming flux at the surface and outgoing flux at the base of the mixed layer. An approximate relationship between heating rate and Q_{pen} can be obtained from Eq. (3). Neglecting the advection and horizontal friction terms, we have:

$$\Delta\frac{\partial T}{\partial t} = -\frac{1}{\rho_0 c_p}\Delta\left[\frac{Q_{pen}(0) - Q_{pen}(-h)}{h}\right], \quad (9)$$

where Δ denotes the difference between K_{var} and K_{const}. In deriving Eq. (9), we assumed the same surface heat fluxes (Eq. (7)) for K_{var} and K_{const}. We also neglected heat diffusion below the mixed layer and the flux across the base of the mixed layer associated with entrainment during mixed-layer deepening. The quantity $\Delta(\partial T/\partial t)$ represents the heating rate attributed to the absorption of solar radiation by phytoplankton. Fig. 9 is a plot of $\Delta(\partial T/\partial t)$ in units of °C per month. At mid-Labrador Sea, the heating rate is very small in winter and spring. It starts to increase rapidly in April, reaching a peak value of 3 °C per month in July. On the Grand Banks, heating starts one month earlier and ends 1 month later than mid-Labrador Sea. The heating rate is high from June to August in spite of the low concentration of chlorophyll during this period. The high heating rate is maintained through the period owing to the small MLD (Fig. 4) as explained in Section 3.1.

The heating rates shown in Fig. 10 are comparable with those found in the Arabian Sea, 4 °C from

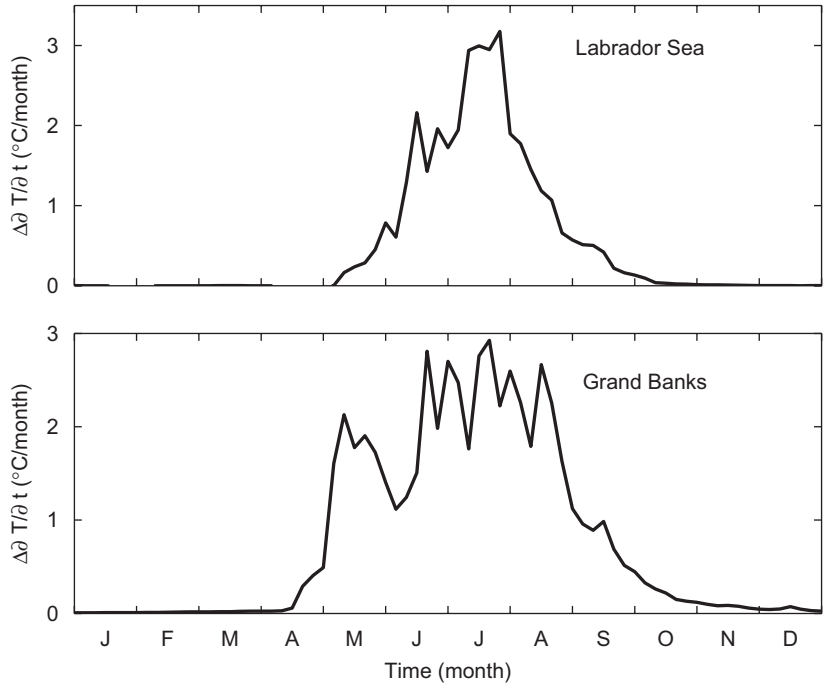

Fig. 10. Difference in solar heating rate for mid-Labrador Sea (upper panel) and the Grand Banks (lower panel) (see Fig. 1 for locations).

August to September (Sathyendranath et al., 1991). They represent the upper limit of temperature increase in the mixed layer for given solar flux and attenuation coefficient. Advection, diffusion and entrainment can reduce the temperature increase considerably from that predicted by (9). Integrating the curve for the Grand Banks from the beginning of April to the end of July, we obtain a temperature difference of 6.2 °C. The actual temperature difference is 2.7 °C according to the numerical model (Fig. 6). The corresponding numbers for mid-Labrador Sea are 4.8 °C (Eq. (9)) and 1.8 °C.

5. Conclusions

In most areas of the Labrador Sea and the adjacent shelves, the effect of bio-optical heating on SST as measured by the SST difference (bio-optical model minus water type model with invariant light attenuation) exceeds 1 °C in summer and fall (July–September) but is negligible in winter and spring. The maximum is on the Grand Banks and Northeastern Newfoundland Shelf where the SST difference reaches 2.7 °C. The SST difference is controlled by both chlorophyll concentration and the MLD.

In areas of high chlorophyll concentration, more irradiance is trapped by chlorophyll within the upper layer and hence less energy is available for heating below the mixed layer. The redistribution of solar radiation in the water column results in cooling of the lower layer. At the Grand Banks the decrease in temperature in the lower layer is about 1.2 °C.

Enhanced surface heating leads to high stratification and thus shallow mixed layers. During the summer months, the MLD from the K_{var} experiment is smaller than that from the constant K_{const} (Water Type I) experiment by 20–50%.

Acknowledgements

The research has been supported by Canadian Space Agency under the Ocean's Pulse (TOP) project and Program for Energy Research and Development (PERD). The authors would like to thank George N. White III for preparing the biological datasets used in this paper. Brendan DeTracey assisted in the setup of the numerical model and provided meteorological data. We thank Brian Petrie and Dave Brickman for their helpful comments and suggestions. This paper derives from

a presentation at the GLOBEC ESSAS Symposium on "Climate variability and Sub-Arctic Marine Ecosystems".

This paper was first presented in the GLOBEC-ESSAS Symposium on "Effects of climate variability on sub-arctic marine ecosystems" hosted by PICES in Victoria, BC, May 2005.

References

Barnier, B., 1998. Forcing the ocean. In: Chassignet, E.P., Verron, J. (Eds.), Ocean Modeling and Parameterization. Kluwer Academic Publishers, The Netherlands, pp. 45–80.

Bird, R.E., 1984. A simple solar spectral model for direct-normal and diffuse horizontal irradiance. Solar Energy 32, 461–471.

Blumberg, A.F., Mellor, G.L., 1987. A description of a three-dimensional coastal ocean circulation model. In: Heaps, N. (Ed.), Three-Dimensional Coastal Ocean Models, vol. 4. American Geophysical Union, Washington, DC, pp. 1–16.

Denman, K.L., 1973. A time-dependent model of the upper ocean. Journal of Physical Oceanography 3, 173–184.

Ezer, T., Mellor, G.L., 2004. A generalized coordinate ocean model and a comparison of the bottom boundary layer dynamics in terrain-following and in *z*-level grids. Ocean Modelling 6, 379–403.

Jerlov, N.G., 1976. Marine Optics. Elsevier, Amsterdam.

Kalnay, E., Kanamitsu, M., Kistler, R., Collins, W., Deaven, D., Gandin, L., Iredell, M., Saha, S., White, G., Woollen, J., Zhu, Y., Chelliah, M., Ebisuzaki, W., Higgins, W., Janowiak, J., Mo, K.C., Ropelewski, C., Wang, J., Leetmaa, A., Reynolds, R., Jenne, R., Joseph, D., 1996. The NCEP/NCAR 40-year reanalysis project. Bulletin of the American Meteorological Society 77, 437–471.

Manizza, M., Le Quere, C., Watson, A.J., Buitenhuis, E.T., 2005. Bio-optical feedbacks among phytoplankton, upper ocean physics and sea-ice in a global model. Geophysical Research Letters 32, doi:10.1029/2004GL020778.

Martin, P.J., 1985. Simulation of the mixed layer at OWS November and Papa with several models. Journal of Geophysical Research 90, 903–916.

McCreary, J.P., Kundu, P.K., 1989. A numerical investigation of sea surface temperature variability in the Arabian Sea. Journal of Geophysical Research 94, 16097–16114.

Mellor, G.L., Kantha, L., 1989. An ice-ocean coupled model. Journal of Geophysical Research 94, 10937–10954.

Morel, A., 1988. Optical modeling of upper ocean in relation to its biogenous matter content (Case I waters). Journal of Geophysical Research 93, 10749–10768.

Nakamoto, S., Kumar, S.P., Oberhuber, J.M., Muneyama, K., Frouin, R., 2000. Chlorophyll modulation of sea surface temperature in the Arabian Sea in a mixed-layer isopycnal general circulation model. Geophysical Research Letters 27, 747–750.

Niiler, P.P., Kraus, E.B., 1977. One-dimensional models of the upper ocean. In: Kraus, E.B. (Ed.), Modeling and Prediction of the Upper Layers of the Ocean. Pergamon Press, Oxford, pp. 143–172.

Paulson, C.A., Simpson, J.J., 1977. Irradiance measurements in the upper ocean. Journal of Physical Oceanography 7, 952–956.

Pope, R.M., Fry, E.S., 1997. Absorption spectrum (380–700 nm) of pure water. II. Integrating cavity measurements. Applied Optics 36, 8710–8723.

Platt, T., Sathyendranath, S., Ravindran, P., 1990. Primary production by phytoplankton: analytic solutions for daily rates per unit area of water surface. Proceedings of the Royal Society of London (B) 241, 101–111.

Platt, T., Woods, J.D., Sathyendranath, S., Barkmann, W., 1994a. Net primary production and stratification in the ocean. Geophysical Monographs 85, 247–254.

Platt, T., Sathyendranath, S., White III, G.N., Ravindran, P., 1994b. Attenuation of visible light by phytoplankton in a vertically structured ocean: solutions and applications. Journal of Plankton Research 16, 1461–1487.

Rochford, P.A., Kara, A.B., Wallcraft, A.J., Arnone, R.A., 2001. Importance of solar subsurface heating in ocean general circulation models. Journal of Geophysical Research 106, 30923–30938.

Sathyendranath, S., Platt, T., 1988. The spectral irradiance field at the surface and in the interior of the ocean: a model for applications in oceanography and remote sensing. Journal of Geophysical Research 93, 9270–9280.

Sathyendranath, S., Platt, T., 1994. New production and mixed-layer physics. Proceedings of the Indian Academy of Sciences-Earth and Planetary Sciences 103, 177–188.

Sathyendranath, S., Platt, T., 1997. Analytic model of ocean color. Applied Optics 36, 2620–2629.

Sathyendranath, S., Platt, T., 1998. Ocean-color model incorporating transspectral processes. Applied Optics 37, 2216–2227.

Sathyendranath, S., Gouveia, A.D., Shetye, S.R., Ravindran, P., Platt, T., 1991. Biological control of surface temperature in the Arabian Sea. Nature 349, 54–56.

Sathyendranath, S., Cota, G., Stuart, V., Maass, H., Platt, T., 2001. Remote sensing of phytoplankton pigments: a comparison of empirical and theoretical approaches. International Journal of Remote Sensing 22, 249–273.

Shell, K.M., Frouim, R., Nakamoto, S., Somerville, R.C.J., 2003. Atmospheric response to solar radiation absorbed by phytoplankton. Journal Geophysical Research 108 (D15), doi:10.1029/2003JD003440.

Simonot, J.-Y., Dollinger, E., Treut, H.L., 1988. Thermodynamic-biological-optical coupling in the oceanic mixed layer. Journal of Geophysical Research 93, 8193–8202.

Tang, C.L., Wang, C.K., 1996. A gridded data set to temperature and salinity for the northwest Atlantic Ocean. Canada Data Report of Hydrographical Ocean Science 148, 45pp.

Yao, T., Tang, C.L., Peterson, I.K., 2000. Modeling the seasonal variation of sea ice in the Labrador Sea with a coupled multicategory ice model and the Princeton ocean model. Journal of Geophysical Research 105, 1153–1166.